ELSEVIER

Fluid Phase Equilibria 182 (2001) 75–95

FLUID PHASE EQUILIBRIA

www.elsevier.nl/locate/fluid

Saturated vapor pressure through a modified Lennard-Jones equation of state

J.M.V. Machado, M.S. Zabaloy[1], E.A. Macedo*

Laboratory of Separation and Reaction Engineering (LSRE), Departamento de Engenharia Química, Faculdade de Engenharia, Universidade do Porto, Rua Dr. Roberto Frias s/n, 4200-465 Porto, Portugal

Received 5 August 2000; accepted 8 January 2001

Abstract

The study of a Lennard-Jones (LJ)-based model for viscosities led us to concentrate on a recent high-quality pressure–density–temperature LJ equation of state (EOS). The application of LJ-EOSs to real fluids typically requires introducing a temperature dependence on the LJ intermolecular potential parameters. Though this goal has been the matter of previous works, we have found the following problems: (a) relatively low quality of the unmodified LJ-EOS (U-LJ-EOS) used as the basis for real-fluid computations; (b) uncontrolled use of the U-LJ-EOS outside the range of conditions of the supporting molecular simulation data; (c) poor reproduction of the pure-compound critical temperature and/or critical pressure and (d) need of iterative calculations either to compute the vapor pressure at a given temperature or to regress the values of the LJ parameters from experimental data at saturation.

In the present work, we address all these problems, and provide useful equations to compute properties at saturation through non-iterative procedures. These procedures conserve the quality of the output numerical result, in comparison to the corresponding iterative algorithms. We examine a number of options for the LJ temperature dependence. Some of them make possible to represent accurately the vapor pressure, in a wide range of temperature, for non-polar, polar and heavy compounds. We also scrutiny the potential (unwanted) appearance of crossing pressure versus volume isotherms, which can be produced by the introduction of a temperature dependence, and propose a simple test to systematically assess the range of applicability of a chosen temperature dependence. We also illustrate here the effect of a good vapor–pressure reproduction on the prediction of viscosities. © 2001 Elsevier Science B.V. All rights reserved.

Keywords: Model; Equation of state; Method of calculation; Vapor pressure; Lennard-Jones; Viscosity

* Corresponding author. Tel.: +351-22-508-1653; fax: +351-22-508-1674.
E-mail addresses: mzabaloy@plapiqui.edu.ar (M.S. Zabaloy), eamacedo@fe.up.pt (E.A. Macedo).
[1] Permanent address: Planta Piloto de Ingenieria Quimica, PLAPIQUI (UNS-CONICET), Camino La Carrindanga Km 7, 8000 Bahia Blanca, Argentina.

0378-3812/01/$20.00 © 2001 Elsevier Science B.V. All rights reserved.
PII: S0378-3812(01)00383-1

1. Introduction

Models based on molecular theory have a greater potential for describing accurately the physical properties of real fluids. This is due to the microscopic picture of matter associated to these models. Among the available model-fluids used in molecular theory, the Lennard-Jones (LJ) fluid is known to grasp the essential behavior of real substances.

The expression for the LJ intermolecular potential is the following.

$$u(r) = 4\varepsilon\left[\left(\frac{\sigma}{r}\right)^{12} - \left(\frac{\sigma}{r}\right)^{6}\right] \tag{1}$$

where r is the intermolecular distance, u the potential energy, ε the depth of the LJ potential well and σ the LJ separation distance at zero energy. According to Eq. (1), the potential energy shared by two molecules depends on their relative positions as specified by only the coordinate r. This is strictly valid only for spherically symmetric molecules. The intermolecular potential for more complex molecules actually depends on additional coordinates such as angles of orientation [1]. However, for practical reasons, the modeling of physical properties for systems containing complex molecules, has been often based on the properties of the LJ fluid. For instance, Sun et al. [2] presented, for viscosity (among other properties), a method which combines the rough sphere theory with LJ viscosities, and applied it to liquid *n*-alkanes up to *n*-$C_{16}H_{34}$. Reid et al. [3] reviewed estimation methods for low-pressure gas viscosities including a method that, while based on LJ viscosities, is applied to non-spherical polar and non-polar molecules. Sun and Teja [4] have modeled the vapor–liquid equilibria of systems containing polar or elongated molecules using a LJ-EOS with temperature-dependent effective LJ parameters. In this case all the complex interactions taking place between real non-spherical molecules, often with presence of polar or specific intermolecular forces, are lumped into a single pseudo LJ intermolecular potential. This approach is acceptable for engineering calculations and hence we follow it in the present work.

The LJ reduced temperature T^+, reduced pressure P^+, and reduced density ρ^+ are conventionally defined as follows.

$$T^+ = \frac{kT}{\varepsilon} \tag{2}$$

$$P^+ = \frac{P\sigma^3}{\varepsilon} \tag{3}$$

$$\rho^+ = N_A\rho\sigma^3 \tag{4}$$

where k is the Boltzmann's constant, T the absolute temperature, P the absolute pressure, N_A Avogadro's number, ρ the mole density (in, e.g. mol cm^{-3} units). The variable ρ^+ can reach values higher than unity.

A fundamental problem of the LJ fluid is that its practical reduced temperature value at the triple point $T_{r,LJ,tp}$ is normally higher than that of real fluids. Below $T_{r,LJ,tp}$, the LJ fluid, at equilibrium, can be either a solid or a low-density vapor. Hence, at $T_r < T_{r,LJ,tp}$, and for any property, no reference equilibrium LJ value can exist for a real dense fluid. In such a case the user needs to resort to extrapolations. One possibility consists of setting extrapolation schemes based on LJ properties under metastable conditions computed through computer experiments (e.g. molecular dynamics, Monte Carlo). The other option consists of setting extrapolation schemes for LJ equations of state (EOSs), based on the known qualitative behavior that a dense LJ fluid should meet to be realistic. The disadvantage of using properties of a metastable dense LJ

fluid, calculated using molecular simulation, is that more than one metastable condition may be compatible with the adopted values for the degrees of freedom. Hence, we apply here LJ-EOSs extrapolations.

We are presently studying a viscosity model based on a LJ viscosity equation of state (VEOS) [5]. Such a VEOS provides the LJ viscosity as a function of temperature and density. The normal engineering need is to compute viscosities at a given temperature and pressure. Hence, a pressure–temperature–density LJ EOS is required. In the present work we study a high quality LJ-EOS. We use it freely only within the proper temperature–density range and propose suitable extrapolation schemes for calculations falling outside the original range of applicability. As with cubic EOSs, we force the model criticality to occur at the experimental critical temperature and pressure. Such a choice results in a too volatile LJ fluid. Hence, we introduce a temperature dependence into the LJ energy parameter ε, using non-iterative calculations, to improve the vapor pressure description. Our preliminary work had the aim of assessing the potential of using a LJ-based approach for modeling viscosities [6]. In such work, we held constant the LJ parameters and we restricted the use of the working equations to their original ranges of applicability (no extrapolations were allowed).

In summary, for the chosen LJ-EOS the main purposes of this work are: (a) to device a procedure to make possible to compute a reasonable value for the LJ fluid–density at any condition of temperature and pressure, e.g. at reduced temperatures below $T_{r,LJ,tp}$ and (b) to force the model to be consistent with known or accepted values of the pure component vapor pressure, using simple mathematical procedures. Actually, it is not our goal to generate a highly predictive model for the vapor pressure. Rather, we want the chosen LJ-EOS to give both liquid-like and vapor-like roots within the proper pressure range, for a given isotherm, through forcing the vapor pressure reproduction. Some other advantages of this approach are: (1) proper limits reached when the EOS is used for mixtures, or for subcooled liquids or for subcritical superheated vapors; (2) consistency among experimental vapor pressure values and calculated fugacity coefficients, phase densities, enthalpies and other thermodynamic properties at saturation and (3) potential prediction of viscosities from vapor pressures at subcritical temperatures, or possibility of exporting the form of the temperature dependence obtained from vapor pressures to the representation of viscosities.

A flexible temperature dependence carries on the danger of producing crossing pressure versus density isotherms [7]. We also look at this problem in the present work.

2. The PVE/hBH Lennard-Jones equation of state

The first step consists of choosing a high quality LJ EOSs. Kolafa and Nezbeda [8] proposed such an analytical EOS for the LJ fluid. The PVE/hBH LJ-EOS. This EOS is based on a perturbed virial expansion with a theoretically defined temperature-dependent reference hard sphere term. The use of two theoretical terms implies that only a simple empirical correction is required to reach the needed accuracy [8]. This correction demands less parameters than modified Benedict-Webb-Rubin (MBWR) LJ-EOSs or other purely empirical LJ-EOSs (see [9] and references therein). A recent example of a MBWR–LJ-EOS is the one proposed by Sun and Teja [4]. The PVE/hBH LJ-EOS is based on critically assessed computer simulation data from several sources. Mecke et al. [10] confirmed the good quality of this LJ-EOS. The PVE/hBH LJ-EOS is the following.

$$z = \frac{P^+}{\rho^+ T^+} = f_{KN}(\rho^+, T^+) \tag{5}$$

where z is the compressibility factor and f_{KN} a function of ρ^+ and T^+, available in [8]. However, we presented the working equations for f_{KN} more concisely in our recent work [6]. The temperature range of application of Eq. (5) is $0.68 \leq T^+ \leq 10$. The range for ρ^+ is from 0 to the density of the dense LJ fluid in equilibrium with the LJ solid ($\rho^+_{\text{fluid,SFE}}$). The LJ triple point temperature is $T^+_{\text{tp}} = 0.687 \pm 0.004$ [11], therefore we decided to use Eq. (5) in the temperature range $0.7 \leq T^+ \leq 10$. The LJ-EOS used by Sun and Teja [4] has a temperature range of application $0.45 \leq T^+ \leq 6$. Hence, when used for a dense fluid at $T^+ < 0.687$, their LJ-EOS acts as an extrapolation tool. The critical coordinates corresponding to Eq. (5) are the following [8].

$$T^+_c = 1.3396 \tag{6}$$

$$P^+_c = 0.1405 \tag{7}$$

$$\rho^+_c = 0.3108 \tag{8}$$

$$z_c = 0.3375 \tag{9}$$

We have found that, in spite of the non-cubic nature of this EOS, the number of ρ^+ values compatible with given physically meaningful values of T^+ and P^+ never exceeds the number of three, as in the case of semi-empirical cubic EOSs (e.g. [12]), as long as the PVE/hBH LJ-EOS is used within the original range of applicability. At subcritical temperatures, an efficient way to compute the number of ρ^+ values compatible with a given value of P^+ is to locate first the two P^+ local extrema [13]. Using this method, we did not find any problem with regard to root discrimination even at subcritical temperatures very close to the critical one. The LJ-EOS, Eq. (5), cannot be reliably used at $T^+ < 0.68$, as illustrated in Fig. 1, which shows the pressure P^+ as a function of density ρ^+ at two different values of temperature T^+, for Eq. (5). The $T^+ = 0.7$ isotherm has the proper shape. However, the $T^+ = 0.27$ isotherm has an unphysical shape due to the presence of multiple local extrema. The $T^+ = 0.27$ isotherm of Fig. 1 clearly illustrates the potential danger that lies behind the direct use, beyond their original range of validity, of EOSs based on molecular theory.

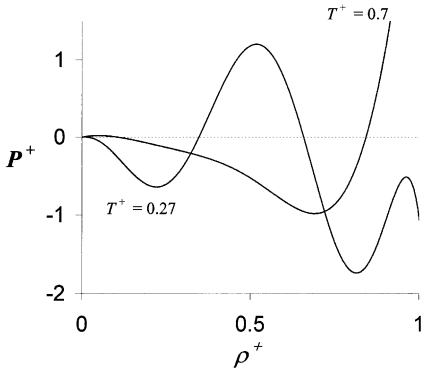

Fig. 1. Lennard-Jones fluid pressure as a function of density at constant temperature according to Eq. (5).

3. Density of the dense LJ fluid in equilibrium with the LJ solid ($\rho^+_{\text{fluid,SFE}}$)

To use Eq. (5) we need to know the value of $\rho^+_{\text{fluid,SFE}}$. Agrawal and Kofke [11] reported properties of the LJ fluid at solid–fluid coexistence from the LJ triple point temperature up to very high temperatures. Agrawal and Kofke [11] provided the following semi-empirical fit of the melting line.

$$P^+_{\text{SFE}} = \beta^{-5/4}(A + B\beta + C\beta^2)\exp(-D\beta^{1/2}) \tag{10}$$

with

$$\beta = \frac{1}{T^+} \tag{11}$$

where P^+_{SFE} is the melting pressure P^+. The parameters of Eq. (10) are the following [11]: $A = 16.89$, $B = -7.19$, $C = -3.028$ and $D = 0.4759$. Eq. (10) corresponds both to the solid–liquid equilibrium and to the solid-supercritical fluid equilibrium. Eq. (10) is not valid for the LJ solid–vapor equilibrium that takes place at temperatures lower than the LJ triple point temperature. The range of Eq. (10) is $0.00365 \leq \beta \leq 1.456$, which corresponds to the (wide) T^+ range $0.686813 \leq T^+ \leq 273.973$. A reliable method to compute $\rho^+_{\text{fluid,SFE}}$ at a given value of T^+ consists of calculating first the pressure of LJ solid/dense–fluid equilibrium P^+_{SFE} using Eq. (10). The resulting value of P^+ is then introduced into Eq. (5) to obtain $\rho^+_{\text{fluid,SFE}}$ (in case of more than one root, the highest density root should be chosen). The ρ^+ values obtained in this way, for the T^+ range of Eq. (5), agree very well [6] with the values of $\rho^+_{\text{fluid,SFE}}$ reported by Agrawal and Kofke [11]. The density $\rho^+_{\text{fluid,SFE}}$ increases with T^+, reaching a value of the order of 1.5 at $T^+ = 10$.

4. Consistency tests and extrapolation schemes

The pressure of an homogeneous fluid held at constant volume increases with temperature. A given EOS violates this fundamental restriction whenever different pressure versus density isotherms intersect each other. The potential appearance of this problem is often studied by generating plots, or not studied at all. A more suitable way of assessing the EOS consistency is to look at the sign of the derivative of pressure P with respect to temperature T, at constant density ρ, in a wide enough region of the $T - \rho$ plane. For constant values of ε and σ, the consistency requirement for the PVE/hBH LJ-EOS can be written as follows.

$$\left(\frac{\partial P^+}{\partial T^+}\right)\bigg|_{\rho^+} > 0 \quad \text{for} \quad \rho^+ > 0 \tag{12}$$

We define ρ^+_∞ as the finite density value at which pressure tends to +infinity ($+\infty$) in Eq. (5). The inverse of ρ^+_∞ is conventionally called 'covolume'. For $0.7 \leq T^+ \leq 10$, it can be shown that ρ^+_∞ is roughly equal to 1.65–2.1 times $\rho^+_{\text{fluid,SFE}}$, depending on the value of T^+. We calculated the above derivative using Eq. (5) at grid points belonging to the domain $0.7 \leq T^+ \leq 10$ and $0 < \rho^+ < \rho^+_\infty$ and did find violations within most of the region defined by the range $\rho^+_{\text{fluid,SFE}} < \rho^+ < \rho^+_\infty$. Fortunately, no violations at all were found within the (proper) density range $0 < \rho^+ \leq \rho^+_{\text{fluid,SFE}}$. The grid steps used were $\Delta T^+ = 0.1$ and $\Delta\rho^+ = 0.01$. We computed the derivative of restriction (12) using finite differences.

5. Scheme for pressure extrapolations in density

Within the temperature range of Eq. (5) calculations for real fluids may require to compute the pressure at a density exceeding the value of $\rho^+_{\text{fluid,SFE}}$ without violating restriction (12). Defining the function h_{KN} as

$$h_{\text{KN}}(\rho^+, T^+) = P^+ = \rho^+ T^+ f_{\text{KN}}(\rho^+, T^+) \tag{13}$$

we set the following linear extrapolation scheme, which defines the function $g(\rho^+, T^+)$

$$\begin{cases} \text{for} \quad 0.7 \le T^+ \le 10 \\ P^+ = g(\rho^+, T^+) = \begin{cases} h_{\text{KN}}(\rho^+, T^+) & \text{for } \rho^+ \le \rho^+_{\text{fluid,SFE}} \\ h_{\text{KN}}(\rho^+_{\text{fluid,SFE}}, T^+) + [\rho^+ - \rho^+_{\text{fluid,SFE}}](h'_{\text{KN}})_{\rho^+_{\text{fluid,SFE}}} & \text{for } \rho^+ > \rho^+_{\text{fluid,SFE}} \end{cases} \end{cases} \tag{14}$$

where $(h'_{\text{KN}})_{\rho^+_{\text{fluid,SFE}}}$ is the partial derivative $\partial h_{\text{KN}}/\partial \rho^+$ evaluated at T^+ and at $\rho^+ = \rho^+_{\text{fluid,SFE}}$.

Note that the above scheme is such that a finite value of density at which pressure tends to infinity does not exist, and hence no 'covolume' is associated to Eq. (14). To make a meaningful comparison against the extrapolation-free original Eq. (5), we tested restriction (12), using Eq. (14), within the same (T^+, ρ^+) grid previously described. We found no violations at all, even at extremely high densities, thus demonstrating the suitability of the above linear extrapolation scheme.

6. Scheme for pressure extrapolations in temperature

For calculations at temperatures outside the range $0.7 \le T^+ \le 10$, we set the following extrapolation equations.

$$P^+ = P^+_{\text{ref}} + \rho^+(T^+ - T^+_{\text{ref}}) \quad \text{with} \quad T^+_{\text{ref}} = \begin{cases} 0.7 & \text{for} \quad T^+ < 0.7 \\ 10 & \text{for} \quad T^+ > 10 \end{cases} \tag{15}$$

where

$$P^+_{\text{ref}} = g(\rho^+, T^+_{\text{ref}}) \tag{16}$$

From Eq. (15), it is clear that the pressure versus density isotherms in the range $\{T^+ < 0.7$ and $T^+ > 10\}$ are totally determined by the $T^+ = 0.7$ isotherm and the $T^+ = 10$ isotherm. Hence, no calculations of $\rho^+_{\text{fluid,SFE}}$ are required outside the range $0.7 \le T^+ \le 10$. Eq. (15) corresponds to assuming that the residual pressure $\lfloor P^+ - \rho^+ T^+ \rfloor$ is independent of temperature for T^+ beyond T^+_{ref}, and equal to the residual pressure $[P^+_{\text{ref}} - \rho^+ T^+_{\text{ref}}]$ at T^+_{ref} and ρ^+. The word 'residual' implies here the difference between the LJ pressure and the ideal gas pressure ($P^+_{\text{ideal gas}} = \rho^+ T^+$) at fixed temperature and density. Since the original PVE/hBH LJ-EOS gives the ideal gas law at low density, the extrapolation scheme (15) has the same behavior. The coupled Eqs. (14) and (15) cover all possible (T^+, ρ^+) conditions. We studied restriction (12) for the coupled Eqs. (14) and (15), in the rectangular wide-ranging domain $0.01 \le T^+ \le 20$ and $0 < \rho^+ \le 2.6$. We found no violations, thus confirming the suitability of the coupled Eqs. (14) and (15). Actually, the extrapolation scheme (15) is such that the pressure P^+ is proportional to the temperature T^+. Hence, by construction, the model avoids the problem of crossing isotherms, in the

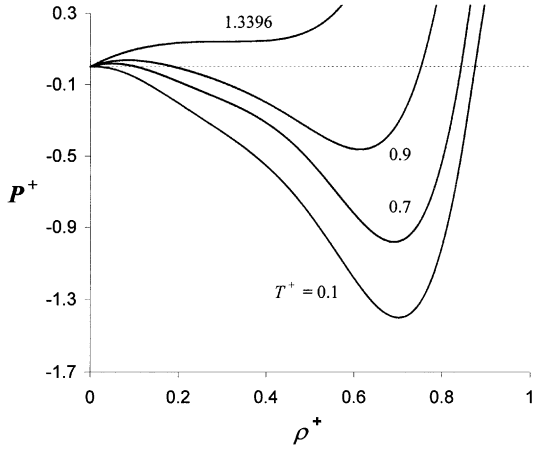

Fig. 2. Pressure as a function of density at constant temperature for the EXT-EJ-EOS.

temperature range $\{T^+ < 0.7$ and $T^+ > 10\}$. Appendix A provides more details on scheme (15). We inspected the shape of pressure versus density isotherms generated using scheme (15) at low temperatures ($T^+ < 0.7$). The isotherms had the proper shape showing a low-density local maximum in pressure and a high-density local minimum, confirming the right qualitative behavior of scheme (15).

The combined schemes (14) and (15) make possible to compute a LJ value of P^+ at any positive values of T^+ and ρ^+, keeping a tight control on the model qualitative behavior at low and supercritical temperatures. The present extrapolation strategy should be preferred to the blind extrapolation of Eq. (5) outside the range of the supporting LJ molecular simulation data.

The set of Eqs. (5), (13)–(16) defines a LJ model that we call EXT-LJ-EOS. Fig. 2 shows pressure versus density isotherms for the EXT-LJ-EOS. The $T^+ = 0.1$ isotherm falls outside the original temperature range of Eq. (5), but due to the extrapolation scheme (15), it has a proper shape. The EXT-LJ-EOS is not really as complicated as it might look at first sight. It can be easily programmed in a computer and it is well-behaved. The core equation of the EXT-LJ-EOS is the PVE/hBH EOS, i.e. Eq. (5), which has an algebraic form necessarily more complicated than simple cubic EOS, because it is aimed to reproduce results from computer experiments. This is the price to be paid for switching from more empirical EOSs to EOSs based on molecular theory, together with the need of having to set extrapolation schemes. With the current availability of fast and relatively inexpensive computers, algebraic complexity is not really an issue, as long as the model is well behaved.

7. Saturated vapor pressure with the EXT-LJ-EOS

Eqs. (14) and (15) completely define the EXT-LJ-EOS relation among P^+, ρ^+ and T^+, at any possible (T^+, ρ^+) condition. From such relation and from exact thermodynamics, the expression for the fugacity coefficient φ can be found. Careful attention should be paid to the proper introduction of the extrapolation equations within the expression for φ. We tested our codes for φ, in all (four) (T^+, ρ^+) regions of Eqs. (14) and (15), through numerical differentiation according to [14]. We obtained the saturated vapor pressure $P^{+,\mathrm{sat}}$, in a wide temperature range, by solving the isofugacity condition for the pure LJ fluid. Since the integration variable is the density, within the (not shown) expression for φ, the results are valid both

Table 1
Sample results for the saturated vapor pressure computed using the EXT-LJ-EOS

T^+	0.05	0.15	0.25	0.5	0.75
$P^{+,\mathrm{sat}}$	1.2810×10^{-33}	1.9946×10^{-12}	4.6963×10^{-8}	1.2445×10^{-4}	2.6241×10^{-3}
T^+	0.95	1.1	1.3	1.3395	
$P^{+,\mathrm{sat}}$	1.7478×10^{-2}	4.5857×10^{-2}	1.1972×10^{-1}	1.4045×10^{-1}	

for constant and/or for temperature-dependent values of ε and σ. We stress that, if ε and σ are made temperature-dependent, then Eq. (32) of [8] for the LJ internal energy becomes invalid. Table 1 shows some of the computed values.

For $0.7 \leq T^+ \leq T_c^+$ our computations agree well with those which Mecke et al. [10] reported for the PVE/hBH LJ-EOS. We extended the calculation up to extremely low values of T^+ in order to use the model for compounds, such as propane, having an extremely low ratio between the triple point pressure and temperature. At this point, it is important to remark that it is better to write the expression for φ in terms of T^+ and the compressibility factor z, rather than in terms of T^+ and ρ^+, mainly if calculations at very low temperature have to be carried out.

Following Soave [15] we correlated $P^{+,\mathrm{sat}}$ as a function of T^+, and also the inverse function, to perform further vapor pressure calculations or parameter regressions in a non-iterative way. The results are the following.

$$Y = F_{\mathrm{dir}}(X) \tag{17}$$

$$X = F_{\mathrm{inv}}(Y) \tag{18}$$

where

$$Y = \frac{P^*}{T^*} \tag{19}$$

$$X = \frac{1}{T^*} \tag{20}$$

$$P^* = \frac{P^+}{P_c^+} \tag{21}$$

$$T^* = \frac{T^+}{T_c^+} \tag{22}$$

We define the explicit functions F_{dir} and F_{inv} in Appendix B. The correlation error associated with functions F_{dir} and F_{inv} is low enough to make possible to replace iterative calculations by explicit calculations. Eq. (17) makes possible to calculate saturated vapor pressures explicitly, while Eq. (18) is useful for parameter regression and/or for setting a temperature dependence for the LJ ε parameter, non-iteratively, as shown below.

The functions F_{dir} and F_{inv} in Appendix B depend on a number of parameters. However, these parameters are general for the EXT-LJ-EOS, i.e. they are not compound-specific. Appendix B parameters have the sole purpose of replacing iterative calculations by explicit calculations without loss of quality in the output result. The modeling potential of the EXT-LJ-EOS is obviously independent on the calculation method

chosen for computing vapor pressures. Hence, the user may completely ignore, if he/she wants, the information available in Appendix B when calculating a pure-compound vapor pressure for the EXT-LJ-EOS, and use instead any method for solving the necessary condition of equilibrium written for the EXT-LJ-EOS. However, that would be impractical. To fix ideas, it is much easier and faster to calculate a vapor pressure, for the present non-cubic EXT-LJ-EOS, using the direct procedure represented by Eq. (17), than calculating a vapor pressure for a simpler empirical EOS using the conventional iterative procedures.

When using the one fluid approach, i.e. for mixture parameters which are composition weighed averages of the pure compound parameters, the relationship among T^+, P^+ and ρ^+ is assumed to be the same than the one valid for the pure compounds. In such a case, Eq. (17) can be used, within EXT-LJ-EOS computer codes for mixtures, to quickly locate a pressure value for which liquid- and vapor-like roots exist.

8. Introducing a temperature dependence into the EXT-LJ-EOS

In this work we chose to obtain the critical values of ε and σ, i.e. ε_c and σ_c, from Eqs. (2), (3), (6) and (7) used with the experimental values of the critical temperature T_c and of the critical pressure P_c. Thus, the experimental critical T, P coordinates are exactly reproduced as in the case of cubic EOSs. We discussed the advantages of this choice elsewhere [6]. Sun and Teja [4] did not force such a reproduction, and hence criticality corresponded in their work to T_c and P_c values different from the experimental ones. If ε and σ are set to be constant and, respectively, equal to ε_c and σ_c, then the predicted vapor pressure becomes too high, mainly at low temperatures. Hence, it is necessary to introduce a proper temperature dependence for these parameters.

From Eq. (2) the following equation can be derived.

$$\frac{T^+}{T_c^+} = \frac{T_r}{\alpha_\varepsilon}$$

where

$$T_r = \frac{T}{T_c} \tag{24}$$

$$\alpha_\varepsilon = \frac{\varepsilon}{\varepsilon_c} \tag{25}$$

If ε does not depend on temperature, then the variable α_ε is equal to unity. As in [4] we held σ constant with temperature and equal to σ_c. Hence, from Eq. (3) it can be shown that

$$\frac{P^+}{P_c^+} = \frac{P_r}{\alpha_\varepsilon}$$

where

$$P_r = \frac{P}{P_c} \tag{27}$$

Combining Eqs. (17), (23) and (26), we write

$$\frac{P_r}{T_r} = F_{dir}\left(\frac{\alpha_\varepsilon}{T_r}\right) \tag{28}$$

If α_ε is known as a function of temperature, Eq. (28) makes possible to compute explicitly the vapor pressure at saturation for a given temperature, using the EXT-LJ-EOS. Combining Eqs. (18), (23) and (26), we write

$$\frac{\alpha_\varepsilon}{T_\mathrm{r}} = F_\mathrm{inv}\left(\frac{P_\mathrm{r}}{T_\mathrm{r}}\right) \tag{29}$$

Eq. (29) makes possible to regress from a experimental vapor pressure data point the value of α_ε that reproduces exactly the experimental vapor pressure. Soave [15], Zabaloy and Vera [12], and Sacomani et al. [16] used relations such as Eqs. (28) and (29) for the case of cubic EOSs.

Let us assume that the temperature dependence of the vapor pressure of a pure compound is known.

$$P_\mathrm{r}^\mathrm{sat} = f_0(T_\mathrm{r}) \tag{30}$$

where $f_0(T_\mathrm{r})$ is a known explicit analytical function of T_r which represents well the vapor pressure curve (VPC) of the chosen pure compound, either through generalized parameters or through compound-specific parameters. The function (30) can be directly introduced into Eq. (29) to define the temperature dependence of α_ε. Then, if the result is introduced into Eq. (28), the back calculated pressure will be virtually equal to the value obtained with Eq. (30) due to the low error associated to the functions F_dir and F_inv. This technique is somehow an hybrid between the techniques used in [12,16] for cubic EOSs. What is gained by the user, who obtains the α_ε temperature dependence as described, is to force the EXT-LJ-EOS to be fully consistent with the known experimental pure-compound vapor pressure. We already discussed in the introduction the advantages of such situation. The practical fact here is that we get vapor–pressure consistency without having to resort to iterative calculations. Hence, for the chosen compound, the vapor–pressure-consistent analytical (explicit) form for α_ε is the following.

$$\alpha_\varepsilon = T_\mathrm{r} F_\mathrm{inv}\left[\frac{f_0(T_\mathrm{r})}{T_\mathrm{r}}\right] \tag{31}$$

When using Eq. (31) the quality in the vapor pressure representation achieved by the EXT-LJ-EOS is the same than the original quality of $f_0(T_\mathrm{r})$. The difference is that the EXT-LJ-EOS can be used to calculate many thermodynamic properties, while the function $f_0(T_\mathrm{r})$, if not coupled to the EXT-LJ-EOS, is limited to only one property: the vapor pressure. Eq. (31) sets the α_ε temperature dependence from information at saturation. The result is then used for calculations using Eqs. (14), (15), (23), (26) and (31) at any condition (saturation or not), as long as the temperature does not exceed the critical one. This is the conventional chemical engineering approach. For temperatures higher than the critical Eq. (31) should not be used. The user may set $\varepsilon = \varepsilon_\mathrm{c}$ and $\sigma = \sigma_\mathrm{c}$ at temperatures higher than T_c or get their temperature dependence from another property, measured at supercritical temperatures.

9. Real fluids: forms for the α_ε temperature dependency

We used the pure-compound DIPPR database [17] as our source of the following experimental data: T_c, the triple point temperature T_tp, and the VPC [$P_\mathrm{r}^\mathrm{sat} = f_\mathrm{DIPPR}(T_\mathrm{r})$] in the range [$T_\mathrm{tp}$, T_c]. For full consistency, using the DIPPR–VPC, we obtained: (a) the vapor pressure at the triple point $P_\mathrm{tp}^\mathrm{sat}$ as f_DIPPR at T_tp; (b) P_c as f_DIPPR at T_c and (c) the acentric factor ω and the boiling point temperature T_b, from their definitions and from f_DIPPR. We used a database of more than 100 compounds of varied nature.

We studied a few forms for $f_0(T_r)$ that we introduced into Eq. (31). In all cases we inspected the following restriction.

$$\left(\frac{\partial P_r}{\partial T_r}\right)\bigg|_{\rho} = \left(\frac{\partial P_r}{\partial T_r}\right)\bigg|_{\rho^+} > 0 \quad \text{for} \quad \rho > 0, \quad (\rho^+ > 0) \tag{32}$$

From the fact that the EXT-LJ-EOS does not violate restriction (12) in a wide (T^+, ρ^+) domain we cannot conclude that restriction (32) will be automatically satisfied. Compliance with restriction (12), which is written in terms of dimensionless variables, guaranties the satisfaction of constraint (32) only for constant LJ parameters. Hence, for temperature dependent LJ parameters restriction (32) should be checked. Note that since, in this work, we set σ constant with temperature and equal to σ_c, from Eq. (4), it is clear that constant ρ implies constant ρ^+. For this test, we used a grid corresponding to $T_{r,tp} \leq T_r \leq 1$ and to $0 < \rho^+ \leq 2.6$, where $T_{r,tp} = T/T_{tp}$. The steps were $\Delta T_r = \lfloor (1 - T_{r,tp})/40 \rfloor$ and $\Delta\rho^+ = 0.025$. The first case we studied was

$$f_0(T_r) = f_{DIPPR}(T_r) \tag{33}$$

which obviously made possible to exactly reproduce the DIPPR vapor pressure values from T_{tp} to T_c using Eqs. (28) and (31).

The second set of cases corresponded to the following equation.

$$f_0(T_r) = \exp\left\lfloor \kappa_1(T_r^{-1} - 1) + \kappa_2 \ln T_r + \kappa_3(T_r - 1) \right\rfloor \tag{34}$$

Eq. (34) can be derived from assuming a quadratic dependence in temperature for the heat of vaporization, integrating the Clapeyron equation using usual assumptions, and setting $P_r = 1$ for $T_r = 1$. The hierarchy of κ_1 is higher than that of κ_2, and the hierarchy of κ_2 is higher than that of κ_3. This is because κ_1, κ_2 and κ_3 correspond, respectively, to the independent term (C), the linear (L) term and the quadratic (Q) term of the assumed quadratic dependence for the heat of vaporization. Hence, the only possibilities that should be considered for Eq. (34) are: C: ($\kappa_1 \neq 0, \kappa_2 = \kappa_3 = 0$), L: ($\kappa_1 \neq 0, \kappa_2 \neq 0, \kappa_3 = 0$) and Q: ($\kappa_1 \neq 0, \kappa_2 \neq 0, \kappa_3 \neq 0$). The κ_i coefficients can be adjusted from vapor pressure data, or obtained analytically from three (or less) selected vapor pressure data points. In all cases we evaluated the κ_i coefficients analytically. For case C, we obtained κ_1 from Eq. (34) and from the acentric factor (ω) definition, being the result $\kappa_1 = (-7/3)(1 + \omega)\ln 10$. This is option Cw. For case L we calculated κ_1 and κ_2 from ω and from the triple point vapor pressure (T_{tp}, P_{tp}^{sat}) (option LwTP). For case Q we computed κ_1, κ_2 and κ_3 from ω, from the boiling point T_b and from (T_{tp}, P_{tp}^{sat}) (option QwTPTb). To quantify the κ_i coefficients we analytically solved a $1 \times 1/2 \times 2/3 \times 3$ linear system of equations, based on Eqs. (30) and (34), for the case C/L/Q. Depending on the particular problem, the user may select other vapor pressure data points.

The form of function $f_{DIPPR}(T_r)$ is similar to that defined by Eq. (34). The difference is in the last term within the exponential argument, which is linear for Eq. (34) and is proportional to a compound-specific integer power of temperature for $f_{DIPPR}(T_r)$. For most of the cases studied here such power is greater than unity.

From the calculated κ_i coefficients we computed the EXT-LJ-EOS vapor pressure from the triple point temperature up to the critical temperature using Eqs. (28), (31) and (34).

Table 2 shows the interpolation/extrapolation accuracy in vapor pressure for options Cw, LwTP and QwTPTb. Table 2 also reports ranges of conditions at which the EXT-LJ-EOS violates restriction (32). This is shown for options Cw, LwTP and QwTPTb, and also for the case $f_0(T_r) = f_{DIPPR}(T_r)$.

Table 2
Comparison between experimental (DIPPR) vapor pressures and vapor pressures computed with the EXT-LJ-EOS[a]

Compound	Vapor pressure description						Information on ranges of violation to constraint (32) within the temperature range from T_{tp} to T_c											
	Temperature range: $T_r > 0.6$		Temperature range from T_{tp} to T_c				Cw			LwTP			QwTPTb			DIPPR		
	Cw AAD%	Cw max AD%	LwTP AAD%	LwTP max AD%	QwTPTb AAD%	QwTPTb max AD%	Minimum T_r	Minimum T_r	Minimum P_r	Minimum T_r	Maximum T_r	Minimum P_r	Minimum T_r	Maximum T_r	Minimum P_r	Minimum T_r	Maximum T_r	Minimum P_r
Hydrogen	3	9	1	1	0.04	0.2	0.42	0.46	14.3	0.43	0.43	21.0	0.43	0.43	21.0	0.42	0.43	21.0
Hydrogen (*para*)	3	8	1	1	0.2	0.4	0.42	0.46	14.2	0.42	0.43	21.0	0.42	0.43	21.0	0.42	0.43	21.0
Nitrogen	1	2	1	2	0.1	0.3	0.50	0.54	13.5	0.50	0.54	13.5	0.50	0.54	10.3	0.50	0.54	10.3
Oxygen	1	2	3	7	0.3	2	0.35	0.53	13.4	0.35	0.55	10.3	0.35	0.53	10.2	0.35	0.53	10.2
Neon	2	4	1	2	0.3	1	b	b	b	b	b	b	b	b	b	b	b	b
Chlorine	1	3	2	5	0.2	1	0.41	0.54	13.7	0.41	0.56	10.6	0.41	0.56	10.6	0.41	0.56	10.6
Argon	1	2	1	2	0.1	0.2	b	b	b	b	b	b	b	b	b	b	b	b
Bromine	2	3	3	6	0.1	0.2	0.46	0.56	10.7	0.46	0.56	10.8	0.46	0.56	10.8	0.46	0.56	10.8
Iodine	2	4	3	5	0.4	1	0.47	0.56	10.7	0.47	0.56	10.7	0.47	0.56	10.7	0.47	0.56	10.7
Ammonia	1	4	2	3	0.04	0.2	0.48	0.60	11.3	0.48	0.60	11.4	0.48	0.60	11.3	0.48	0.60	11.3
Water	1	4	3	6	0.3	1	0.42	0.61	11.6	0.42	0.61	11.7	0.42	0.61	11.7	0.42	0.61	11.7
Hydrogen sulfide	1	2	1	2	0.3	1	0.50	0.55	13.9	0.50	0.56	10.7	0.50	0.56	10.7	0.50	0.56	10.7
Hydrogen chloride	2	3	3	4	0.1	1	0.49	0.57	10.8	0.49	0.57	10.8	0.49	0.57	10.8	0.49	0.57	10.8
Hydrogen iodide	1	2	1	2	0.2	1	0.52	0.55	13.5	0.52	0.55	13.6	0.52	0.55	10.4	0.52	0.55	10.4
Carbon monoxide	1	2	1	2	0.1	0.2	0.51	0.55	13.5	0.51	0.55	13.6	0.51	0.55	10.4	0.51	0.55	10.4
Sulfur dioxide	2	10	1	2	0.3	1	0.46	0.59	11.2	0.46	0.59	11.4	0.46	0.59	11.4	0.46	0.59	11.4
Methane	1	2	1	2	0.1	0.3	0.48	0.53	13.3	0.48	0.53	13.3	0.48	0.53	13.3	0.48	0.53	13.3
Ethane	1	2	6	14	0.6	2	0.30	0.56	10.6	0.30	0.56	10.7	0.30	0.56	10.6	0.30	0.56	10.6
Propane	1	2	10	25	1.4	5	0.23	0.56	10.9	0.23	0.58	11.0	0.23	0.58	6.7	0.23	0.58	6.8
n-Butane	1	4	7	15	0.6	2	0.32	0.57	11.1	0.32	0.59	11.2	0.32	0.59	11.1	0.32	0.59	11.1
n-Pentane	1	6	8	20	0.8	3	0.31	0.58	11.3	0.31	0.60	11.4	0.31	0.60	7.3	0.31	0.60	7.3
n-Hexane	1	6	9	20	0.6	2	0.35	0.59	11.5	0.35	0.61	11.6	0.35	0.61	7.6	0.35	0.61	7.6
n-Heptane	2	11	7	15	0.7	2	0.34	0.60	11.7	0.34	0.62	7.8	0.34	0.62	7.8	0.34	0.62	7.8
n-Octane	2	10	6	12	0.6	1	0.38	0.61	11.9	0.38	0.63	8.0	0.38	0.63	7.9	0.38	0.63	7.9
n-Nonane	3	14	7	15	0.4	1	0.37	0.62	12.0	0.37	0.64	8.2	0.37	0.64	8.1	0.37	0.64	8.1
n-Decane	3	16	6	12	0.6	2	0.39	0.64	12.1	0.39	0.64	8.3	0.39	0.64	8.3	0.39	0.64	8.3
n-Undecane	3	20	7	15	0.5	2	0.39	0.65	12.2	0.39	0.65	8.5	0.39	0.65	8.4	0.39	0.65	8.4
n-Dodecane	3	18	7	14	0.5	2	0.40	0.66	12.4	0.40	0.66	8.6	0.40	0.66	8.5	0.40	0.66	8.5
n-Tridecane	4	22	7	14	0.5	2	0.40	0.65	12.5	0.40	0.67	8.7	0.40	0.65	8.6	0.40	0.65	8.6
n-Tetradecane	5	23	6	13	0.5	1	0.40	0.66	12.6	0.40	0.67	8.7	0.40	0.66	8.7	0.40	0.66	8.7
n-Pentadecane	6	26	6	12	0.5	2	0.40	0.67	12.7	0.40	0.67	8.8	0.40	0.67	8.8	0.40	0.67	8.8
n-Hexadecane	6	27	7	14	0.4	1	0.40	0.67	12.8	0.40	0.67	8.9	0.40	0.67	8.9	0.40	0.67	8.9
n-Heptadecane	6	28	7	14	0.5	2	0.40	0.67	13.0	0.40	0.69	9.0	0.40	0.69	8.9	0.40	0.69	9.0
n-Octadecane	6	30	7	13	0.8	2	0.40	0.69	13.0	0.40	0.69	9.0	0.40	0.69	9.0	0.40	0.69	9.0
Cyclohexane	1	7	2	4	0.4	1	0.51	0.58	11.1	0.51	0.59	11.2	0.51	0.59	11.2	0.51	0.59	11.2
Neopentane	1	5	1	3	0.3	1	b	b	b	b	b	b	b	b	b	b	b	b
Bicyclohexyl	1	6	7	15	0.6	2	0.38	0.63	11.9	0.38	0.63	12.0	0.38	0.63	7.9	0.38	0.63	7.9
Ethylene	1	2	4	9	0.3	1	0.37	0.56	10.5	0.37	0.56	10.7	0.37	0.56	10.6	0.37	0.56	10.6
Propylene	1	4	9	22	1.0	4	0.24	0.56	10.8	0.24	0.58	11.0	0.24	0.56	6.7	0.24	0.56	6.7
Benzene	1	6	3	4	0.2	1	0.50	0.58	11.1	0.50	0.58	11.2	0.50	0.58	11.2	0.50	0.58	11.2
Toluene	1	5	8	18	0.8	3	0.30	0.60	11.3	0.30	0.60	11.5	0.30	0.60	7.4	0.30	0.60	7.4
Ethylbenzene	1	7	10	24	1.1	4	0.29	0.61	11.5	0.29	0.61	7.6	0.29	0.61	7.6	0.29	0.61	7.6
n-Propylbenzene	1	7	11	27	1.2	4	0.27	0.60	11.7	0.27	0.62	7.8	0.27	0.62	7.7	0.27	0.62	7.7
o-Xylene	1	8	5	10	0.3	1	0.39	0.61	11.5	0.39	0.61	11.7	0.39	0.61	11.6	0.39	0.61	11.6
m-Xylene	1	8	6	12	0.5	1	0.37	0.60	11.6	0.37	0.62	11.7	0.37	0.60	7.6	0.37	0.60	7.6
p-Xylene	1	6	3	5	0.2	0.5	0.46	0.61	11.5	0.46	0.61	11.7	0.46	0.61	11.6	0.46	0.61	11.6

1-2-3-Trimethylbenzene	1	8	4	9	0.3	1	0.37	0.61	11.7	0.37	0.62	11.8	0.37	0.62	7.7	0.37	0.62	7.7
Indane	1	6	9	21	0.7	2	0.32	0.59	11.5	0.32	0.61	11.7	0.32	0.61	7.6	0.32	0.61	7.6
Styrene	1	6	7	15	0.5	1	0.38	0.60	11.5	0.38	0.61	11.6	0.38	0.60	7.6	0.38	0.60	7.6
Biphenyl	2	12	4	7	1.0	2	0.44	0.62	11.8	0.44	0.62	12.0	0.44	0.62	8.0	0.44	0.62	11.9
Diphenylmethane	2	13	7	15	0.4	1	0.39	0.64	12.1	0.39	0.64	8.3	0.39	0.64	8.2	0.39	0.64	8.2
Naphthalene	2	8	3	6	0.7	2	0.47	0.60	11.5	0.47	0.60	11.6	0.47	0.60	11.6	0.47	0.60	11.6
1-Methylnaphthalene	3	12	4	9	0.3	1	0.31	0.61	11.6	0.31	0.62	7.7	0.31	0.61	7.7	0.31	0.61	7.7
2-Methylnaphthalene	4	9	10	15	2.6	6	0.40	0.61	11.8	0.40	0.63	11.9	0.40	0.61	7.8	0.40	0.61	7.8
Phenanthrene	2	8	5	8	1.2	3	0.43	0.63	12.1	0.43	0.64	12.1	0.43	0.63	8.1	0.43	0.63	8.1
Dimethyl ether	1	4	4	8	1.4	3	0.33	0.58	11.1	0.33	0.58	11.2	0.33	0.58	11.1	0.33	0.58	11.1
Methyl ethyl ether	3	25	16	33	0.9	3	0.37	0.59	11.2	0.37	0.60	8.0	0.37	0.60	7.8	0.37	0.60	7.8
Diethyl ether	1	9	9	22	0.01	0.03	0.34	0.60	11.4	0.34	0.60	7.6	0.34	0.60	7.6	0.34	0.60	7.6
Methyl *n*-propyl ether	3	13	2	5	1.0	3	0.28	0.59	11.3	0.28	0.60	7.4	0.28	0.60	7.4	0.28	0.60	7.4
Methyl isopropyl ether	2	9	6	13	2.4	8	0.28	0.60	11.4	0.28	0.60	7.4	0.28	0.60	7.4	0.28	0.60	7.4
Methyl *n*-butyl ether	2	5	12	27	1.3	4	0.31	0.60	11.6	0.31	0.62	7.7	0.31	0.60	7.6	0.31	0.60	7.7
Methyl *tert*-butyl ether	1	7	5	9	1.6	4	0.33	0.60	11.3	0.33	0.60	11.5	0.33	0.60	7.4	0.33	0.60	11.4
Ethyl propyl ether	3	6	20	45	2.2	8	0.29	0.61	11.6	0.29	0.61	8.0	0.29	0.61	7.7	0.29	0.61	7.8
Di-*n*-propyl ether	2	8	9	19	4.0	13	0.28	0.61	11.7	0.28	0.62	7.8	0.28	0.62	7.7	0.28	0.62	7.8
Di-isopropyl ether	3	9	0.3	1	0.1	0.4	0.38	0.61	11.6	0.38	0.61	11.7	0.38	0.61	11.7	0.38	0.61	11.7
Acetone	1	6	5	10	0.3	1	0.35	0.59	11.5	0.35	0.61	11.6	0.35	0.61	11.5	0.35	0.61	11.5
Methyl ethyl ketone	1	7	5	11	0.5	1	0.35	0.61	11.6	0.35	0.61	11.7	0.35	0.61	7.6	0.35	0.61	11.6
2-Pentanone	2	10	6	13	0.4	1	0.35	0.61	11.6	0.35	0.61	11.8	0.35	0.61	7.7	0.35	0.61	7.7
3-Pentanone	2	10	1	2	0.4	1	0.42	0.61	11.6	0.42	0.62	11.7	0.42	0.62	11.7	0.42	0.62	11.7
2-Hexanone	2	10	7	16	0.5	2	0.37	0.62	11.8	0.37	0.62	7.9	0.37	0.62	7.9	0.37	0.62	7.9
3-Hexanone	2	10	6	11	1.9	5	0.37	0.62	11.7	0.37	0.62	11.9	0.37	0.62	7.9	0.37	0.62	7.9
3-Heptanone	3	19	5	9	1.4	4	0.39	0.62	11.9	0.39	0.63	8.1	0.39	0.63	8.1	0.39	0.63	8.1
5-Nonanone	3	16	5	9	1.5	4	0.42	0.64	12.2	0.42	0.65	8.4	0.42	0.65	8.3	0.42	0.65	8.3
3-3-Dimethyl-2-butanone	2	10	5	8	1.3	3	0.39	0.60	11.6	0.39	0.62	11.7	0.39	0.60	7.7	0.39	0.60	11.7
Methanol	2	9	6	13	0.4	1	0.34	0.65	12.3	0.34	0.65	8.3	0.34	0.65	8.3	0.34	0.65	8.3
Ethanol	5	20	3	7	0.4	1	0.31	0.65	12.6	0.31	0.65	8.7	0.31	0.65	8.6	0.31	0.65	8.6
1-Propanol	8	35	5	12	0.7	2	0.27	0.66	12.5	0.27	0.66	8.7	0.27	0.66	8.7	0.27	0.66	8.7
1-Butanol	8	35	6	11	2.2	6	0.33	0.65	12.5	0.33	0.66	8.7	0.33	0.66	8.7	0.33	0.66	8.7
1-Pentanol	7	30	11	25	1.0	3	0.33	0.65	12.4	0.33	0.65	8.7	0.33	0.65	8.6	0.33	0.65	8.6
1-Hexanol	8	40	7	13	2.3	6	0.37	0.66	12.4	0.37	0.66	8.7	0.37	0.66	8.6	0.37	0.66	8.6
1-Octanol	7	43	11	18	3.5	9	0.39	0.65	12.4	0.39	0.65	8.7	0.39	0.65	8.6	0.39	0.65	8.7
1-Decanol	8	48	13	25	0.8	3	0.41	0.66	12.5	0.41	0.66	8.8	0.41	0.66	8.7	0.41	0.66	8.7
1-Heptadecanol	6	37	14	26	0.04	0.2	0.42	0.70	13.1	0.42	0.70	9.1	0.42	0.70	9.1	0.42	0.70	9.1
1-Octadecanol	5	36	16	30	0.5	2	0.42	0.70	13.2	0.42	0.70	9.2	0.42	0.70	9.1	0.42	0.70	9.1
Isopropanol	8	33	1	2	0.3	1	0.36	0.67	12.7	0.36	0.67	8.8	0.36	0.67	8.8	0.36	0.67	8.8
2-Methyl-1-propanol	9	39	8	16	3.4	11	0.30	0.65	12.4	0.30	0.65	8.7	0.30	0.65	8.7	0.30	0.65	8.7
2-Butanol	9	37	6	12	2.5	8	0.30	0.65	12.4	0.30	0.65	8.7	0.30	0.65	8.6	0.30	0.65	8.6
2-Methyl-2-propanol	11	53	3	5	0.2	0.5	0.59	0.66	12.5	0.59	0.66	8.7	0.59	0.66	8.7	0.59	0.66	8.7
Acetic acid	2	4	3	6	0.9	2	0.49	0.63	12.1	0.49	0.63	12.1	0.49	0.63	12.1	0.49	0.63	12.1
Propionic acid	4	15	1	1	0.2	0.4	0.42	0.65	12.4	0.42	0.65	8.4	0.42	0.65	8.4	0.42	0.65	8.4
n-Propylamine	4	14	1	3	0.1	0.2	0.38	0.60	11.4	0.38	0.61	11.5	0.38	0.61	11.5	0.38	0.61	11.5
Isopropylamine	2	12	6	14	0.002	0.01	0.38	0.60	11.4	0.38	0.61	11.6	0.38	0.60	7.6	0.38	0.60	7.6
n-Butylamine	2	11	4	6	0.9	2	0.42	0.61	11.6	0.42	0.61	11.8	0.42	0.61	11.7	0.42	0.61	11.7
tert-Butylamine	3	9	1	2	0.002	0.01	0.43	0.60	11.4	0.43	0.60	11.5	0.43	0.60	11.5	0.43	0.60	11.5
sec-Butylamine	1	8	4	9	1.4	4	0.33	0.60	11.4	0.33	0.60	11.6	0.33	0.60	7.4	0.33	0.60	11.5
Isobutylamine	2	9	6	11	1.8	5	0.37	0.62	11.7	0.37	0.62	11.8	0.37	0.62	7.8	0.37	0.62	7.8
Diethylamine	2	11	2	3	0.5	1	0.45	0.60	11.5	0.45	0.61	11.6	0.45	0.60	11.6	0.45	0.60	11.6
Chloroform	1	4	7	15	0.3	1	0.39	0.59	11.2	0.39	0.59	11.3	0.39	0.59	11.2	0.39	0.59	11.2
Methyl chloride	1	2	3	6	0.1	0.4	0.42	0.57	10.9	0.42	0.58	11.0	0.42	0.57	10.9	0.42	0.57	10.9
1-1-Dichloroethane	1	8	4	11	0.3	1	0.34	0.59	11.2	0.34	0.60	11.3	0.34	0.59	11.3	0.34	0.59	11.3
1-2-Dichloroethane	2	4	5	10	0.5	1	0.42	0.60	11.4	0.42	0.61	11.5	0.42	0.60	11.4	0.42	0.60	11.4
Nitromethane	3	6	5	9	1.3	3	0.42	0.61	11.7	0.42	0.62	11.7	0.42	0.61	11.7	0.42	0.61	11.7
m-Nitrotoluene	2	3	6	13	0.4	1	0.39	0.64	12.1	0.39	0.64	12.2	0.39	0.64	8.0	0.39	0.64	8.0

Table 2 (*Continued*)

Compound	Vapor pressure description						Information on ranges of violation to constraint (32) within the temperature range from T_{tp} to T_c											
	Temperature range: $T_r > 0.6$		Temperature range from T_{tp} to T_c				Cw			LwTP			QwTPTb			DIPPR		
	Cw AAD%	Cw max AD%	LwTP AAD%	LwTP max AD%	QwTPTb AAD%	QwTPTb max AD%	Minimum T_r	Minimum T_r	Minimum P_r	Minimum T_r	Maximum T_r	Minimum P_r	Minimum T_r	Maximum T_r	Minimum P_r	Minimum T_r	Maximum T_r	Minimum P_r
o-Nitrotoluene	3	5	7	13	2.2	6	0.37	0.64	12.1	0.37	0.64	12.2	0.37	0.64	8.0	0.37	0.64	8.0
p-Nitrotoluene	3	7	11	21	0.2	1	0.44	0.62	11.9	0.44	0.63	8.2	0.44	0.62	8.1	0.44	0.62	8.1
Anisole	2	9	6	14	0.1	1	0.37	0.60	11.7	0.37	0.62	11.8	0.37	0.62	7.7	0.37	0.62	7.7
Tetrahydrofuran	1	6	6	13	2.0	6	0.30	0.58	11.2	0.30	0.60	11.3	0.30	0.58	7.2	0.30	0.58	11.3
Ethyl acetate	2	13	5	10	1.7	4	0.36	0.62	11.7	0.36	0.62	11.9	0.36	0.62	7.8	0.36	0.62	7.8
Furfural	2	8	4	10	0.2	1	0.35	0.61	11.7	0.35	0.61	11.9	0.35	0.61	7.7	0.35	0.61	7.7
m-Cresol	3	18	6	10	1.7	4	0.40	0.63	12.0	0.40	0.64	8.3	0.40	0.63	8.2	0.40	0.63	8.2
Acetonitrile	1	2	3	6	0.1	0.4	0.42	0.61	11.6	0.42	0.61	11.7	0.42	0.61	11.6	0.42	0.61	11.6
Pyridine	1	7	5	11	0.3	1	0.37	0.59	11.2	0.37	0.59	11.4	0.37	0.59	11.3	0.37	0.59	11.3
N-methylpyrrolidine	1	6	4	9	1.3	4	0.33	0.58	11.2	0.33	0.60	11.3	0.33	0.58	11.3	0.33	0.58	11.3
3-Methoxypropionitrile	3	10	4	9	0.01	0.03	0.33	0.63	12.0	0.33	0.63	8.0	0.33	0.63	8.0	0.33	0.63	8.0
N,*N*-dimethylformamide	2	9	7	15	0.8	2	0.33	0.60	11.6	0.33	0.61	7.7	0.33	0.61	7.6	0.33	0.61	7.6
Hexafluorobenzene	2	11	2	5	0.5	1	0.54	0.62	11.8	0.54	0.63	11.9	0.54	0.63	11.9	0.54	0.63	11.9
Benzothiophene	1	8	4	6	0.9	2	0.40	0.60	11.5	0.40	0.61	11.6	0.40	0.60	11.6	0.40	0.60	11.6

[a] Ranges of violation to constraint (32).

[b] No violations.

For option Cw relative errors in vapor pressure are very high in the low temperature region. We expected this, because the input experimental information for this option corresponds to $T_r = 0.7$, and hence option Cw acts as an extrapolation scheme at low temperatures. Thus, for option Cw, we only report errors for $T_r > 0.6$ in Table 2. Within this restricted temperature range the results are acceptable for most of the compounds (alcohols are an important exception). However, at some conditions, the model violates restriction (32). For option Cw, Table 2 reports errors in vapor pressure for $T_r > 0.6$, and conditions of violation of restriction (32) for the range $[T_{tp}, T_c]$. As an example, consider the case of propane: Table 2 shows that violations to Eq. (32) may only occur, for option Cw, between $T_r = 0.23$ and $T_r = 0.56$, only if the reduced pressure P_r is higher or equal than 10.9.

Table 2 shows that, for all the studied options for the temperature-dependency, the model violates restriction (32) only at high reduced pressures, at relatively low reduced temperatures. Only for three compounds we verified full compliance with constraint (32) (neon, argon, neopentane). From Table 2, the violation reduced-temperature range is not sensitive to the adopted option. Depending on the considered pure compound, the reduced pressure of incipient violation may or may not be sensitive to the chosen option. These results show that the introduction of a temperature dependency, within an EOS, can lead to an inconsistent behavior at some conditions. Such conditions may or may not be relevant, depending on the specific problem to which the user applies the model. For the tested compounds, violations happened always at ρ^+ values higher than 0.9–0.925, for all options considered. The violation ranges in Table 2 could be refined by using a temperature–density grid with higher resolution than the one used here.

We do not report errors in vapor pressure for the case $f_0(T_r) = f_{DIPPR}(T_r)$, because, as expected, the errors were obviously negligible, throughout the complete subcritical temperature range. For option LwTP, the vapor pressure reproduction throughout the subcritical range is good for some compounds and fair for others. On the other hand, as it can be seen from the average and maximum deviations reported in Table 2, the description of vapor pressures is very good for option QwTPTb, i.e. within experimental error for the vast majority of the cases. That was also the case for a relatively recent form of the cubic Peng–Robinson EOS, i.e. the ZVPR–EOS, when used with exactly the same input experimental vapor pressure information of option QwTPTb ('option a' of [12]). The study [12] for the ZVPR–EOS corresponds practically to the same database of the present work. Since our ultimate goal is to model real fluid viscosities based on LJ properties, we are restricted to LJ EOSs, and hence we chose the QwTPTb–EXT-LJ-EOS rather than the 'ZVPR–EOS–option a'. The more involved algebraic form of the QwTPTb–EXT-LJ-EOS in comparison to that of the 'ZVPR–EOS–option a' should not be regarded as an important disadvantage. Nowadays, the amount of required input experimental information is a much more important issue than the algebraic model complexity, since experimental measurements are much more expensive than calculations with computation times typical of routine process simulation and design. Furthermore, there is an evident advantage in using PVT EOSs based on molecular theory, when intending to model transport properties: computer experiments such as molecular dynamics provide not only PVT properties, but also transport properties. Hence, with the aid of EOSs for transport properties fitted against computer experiments data, a natural link arises between transport properties at equilibrium and PVT properties at equilibrium. Such a link does not exist for simpler empirical EOSs.

Note that the described technique does not resort to adjustable parameters. Rather, the κ_i coefficients are obtained analytically, in a way that a unique set of values of the κ_i coefficients is computed from the chosen vapor pressure data points. Hence, the typical problem of multiple possible sets of (adjustable) parameters values, with similar quantitative performance, is here avoided.

The EXT-LJ-EOS can be extended to mixtures using the van der Waals (VW) one-fluid mixing rules studied by Sun and Teja [4] for their LJ-EOS. These researchers [4] found that their LJ + VW EOS could be used to correlate as well as extrapolate mixture data over considerable ranges of temperature and pressure, and also found, on the other hand, that commonly used cubic EOS models were inadequate when extrapolated. Sun and Teja [4] comparisons correspond to EOSs (LJ and Peng–Robinson-like), which for pure compounds were adjusted using vapor pressure experimental data. The systems studied [4] contained molecules of considerable complexity (e.g. water, ethanol, methane, *n*-decane), and the pure-compound LJ parameters were made temperature-dependent. In spite of the non-Lennard-Jonnescity of the studied complex molecules, which were modeled [4] using temperature-dependent effective LJ parameters, Sun and Teja [4] concluded that the predictive power is higher for LJ-based EOSs than for cubic EOSs. The most probable explanation for these conclusions is that LJ EOSs acknowledge the existence of discrete molecules through forced agreement with results from molecular level computer experiments, rather than assuming that fluids have a continuous nature.

The added calculation effort associated to LJ-EOSs in comparison to cubic EOSs should not be regarded as a significant problem due to the ever-increasing power of modern computers.

For a multi-component system, vapor–liquid equilibrium exists if the system temperature is less than the pure-compound critical temperature of at least one of the present components. In this case, the mixture bubble pressure can be accurately described only if the vapor pressure is well reproduced by the EOS for at least the most concentrated components. If the system temperature is close to the critical temperature of a component which is at high concentration, then the model can only be successful in representing the VLE if the experimental critical pure-compound T, P coordinates are properly reproduced. These two features are met by the EXT-LJ-EOS if the techniques described here are applied. From these features and from the high quality of the PVE/hBH EOS used as the basis of the EXT-LJ-EOS, a VLE performance at least comparable to that of [4] should be expected when using the EXT-LJ-EOS coupled to VW one-fluid mixing rules.

10. Effect of reproducing the vapor pressure on the representation of viscosities

Fig. 3 shows the viscosity of propylene at 290 K as a function of pressure in a wide range of pressure. The dashed vertical line corresponds to a pressure equal to 0. Curve A corresponds to the LJ viscosity calculated according to [6], with values of ε and σ set to be constant and respectively equal to ε_c and σ_c. Curve A corresponds to a prediction of viscosity from the values of critical temperature and pressure given for propylene in [18]. The squares correspond to the viscosity data available in [18]. The curve A loop comes from the VW loop of the pressure–density–temperature LJ-EOS. The inset within Fig. 3 shows the low pressure-low viscosity region amplified. We see that the model gives both vapor- and liquid-like viscosities at 290 K. For liquid propylene, curve A is such that the model underpredicts the viscosity at all pressures.

From [17], propylene at 290 K has a reduced temperature $T_r = 0.7947$ and a reduced pressure at saturation $P_r = 0.2049$. Introducing these values into Eq. (29), we obtain the value of α_ε which reproduces exactly the saturation pressure, i.e. $\alpha_\varepsilon = 1.049$. From Eq. (25), we calculate the corresponding value of ε at 290 K and use it to generate curve B of Fig. 3. For that, we use the calculation procedure of [6], but with a value of ε which differs from ε_c. Curve B corresponds to a prediction of viscosity from the vapor pressure of propylene at 290 K and from its values of critical temperature and pressure. We see that, for propylene, forcing the LJ parameters to be consistent with vapor pressure information shifted the model predictions in the right direction improving the model quantitative performance, mainly at high pressures.

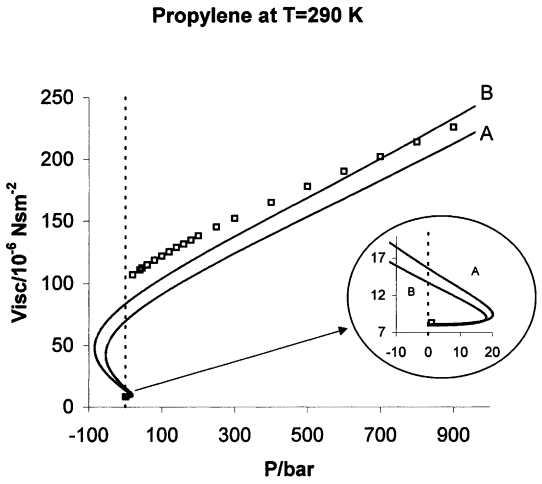

Fig. 3. Predicted viscosity of propylene at 290 K as a function of pressure. Curve A: LJ viscosity calculated according to [6] with $\varepsilon = \varepsilon_c$; curve B: LJ viscosity calculated according to [6] with $\varepsilon = \alpha_\varepsilon \varepsilon_c$ and $\alpha_\varepsilon = 1.049$; (□): Stephan and Lucas [18].

Fig. 3 hence illustrates what we stated in third point of Section 1. We stress that we obtained curves A and B without using any experimental viscosity datum as input or any parameter adjusted from viscosity data.

We obtained Fig. 4 for di-chloro–di-fluoro-methane in a similar way than Fig. 3. The dashed vertical line corresponds to the pressure of the experimental viscosity datum identified with an arrow, i.e. to 20 bar. From [17], di-chloro–di-fluoro-methane has at $T = 360$ K, a reduced temperature $T_r = 0.9352$ and a reduced pressure at saturation $P_r = 0.6378$, which corresponds to $\alpha_\varepsilon = 1.0193$ (Eq. (29)). We observe that forcing consistency with the vapor pressure again shifted the model predictions in the right

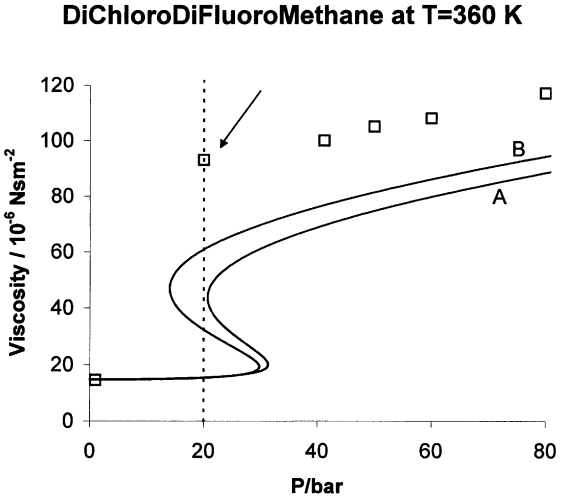

Fig. 4. Predicted viscosity of di-chloro–di-fluoro-methane at 360 K as a function of pressure. Curve A: LJ viscosity calculated according to [6] with $\varepsilon = \varepsilon_c$; curve B: LJ viscosity calculated according to [6] with $\varepsilon = \alpha_\varepsilon \varepsilon_c$ and $\alpha_\varepsilon = 1.0193$; (□): Stephan and Lucas [18].

direction. However, in this case additional corrections to the LJ reference model will be required for reaching a better quantitative performance. Curve A is such that at 20 bar, the model gives only one root which corresponds to a vapor phase. On the other hand, curve B gives three roots at 20 bar. One of them corresponds to a liquid. Hence, forcing consistency with the vapor pressure produced the appearance of a liquid-like viscosity value which corresponds to the situation found experimentally.

11. Conclusions

This work addressed the need to compute LJ densities as a function of temperature and pressure, in wide ranges of temperature and pressure, for further use in LJ-based viscosity calculations. To that end we chose a high-quality LJ-EOS, which has, as any other LJ-EOS, the limitations imposed by the LJ fluid itself, rather than by the chosen LJ-EOS. An important limit is that the LJ (practical) reduced temperature at the triple point is higher than that of real fluids. Hence, we proposed here an extrapolation scheme that makes possible to compute LJ densities or pressures at lower temperatures. We also looked at the density range of applicability of chosen LJ-EOS and set a linear extrapolation scheme with proper qualitative behavior, for computations at high density. We call the original LJ-EOS coupled to our extrapolation schemes EXT-LJ-EOS. We computed, for the EXT-LJ-EOS, the dimensionless vapor pressure at saturation in an extremely wide temperature range, once for all, and correlated the results to make possible either to compute LJ vapor pressures, or to regress parameters from experimental data, avoiding iterative calculations. We exploited this result to make the EXT-LJ-EOS temperature dependence reproduce well experimental vapor pressures. For that, we analytically obtained the needed parameters from a few selected vapor pressure data points. We conclude that, it is possible to achieve a very good description of the pure-compound VPC for substances of diverse nature using the EXT-LJ-EOS. However, all the options we studied did produce violations to the requirement which states that different pressure versus density isotherms should not intersect each other. Violations occurred only at relatively high reduced pressures. The constraint we studied here is restriction (32). It should be inspected in a wide enough temperature–density range whenever a temperature dependence is imposed on an EOS, regardless the nature of the EOSs. The test is simple, and could be added to the set of modern standard tests available in the literature [14,19]. Compliance with restriction (32) for pure compounds does not guarantee compliance for mixtures when using, e.g. temperature dependent interaction parameters or, e.g. temperature dependent mixture covolume parameters. Besides, restriction (32) could be embedded into constrained optimization computer programs used to fit pure compound or mixture parameters from experimental data. Within such programs, restriction (32) should be evaluated not only at the conditions of the experimental data, but also within a wide-ranging temperature–density grid. We stress that the danger of introducing a temperature dependence into EOSs is not only limited to temperature-dependent volume translations: any proposed EOS temperature dependence can potentially violate constraint (32). Finally, we illustrated that a better representation of vapor pressures has a good impact on the LJ based prediction of viscosities.

List of symbols

AAD%	average absolute-value percent relative deviation $= (100/\mathrm{NP})\sum_{i=1}^{\mathrm{NP}} \lvert P_{\mathrm{model}}^{\mathrm{vap}} - P_{\mathrm{exp}}^{\mathrm{vap}} \rvert / P_{\mathrm{exp}}^{\mathrm{vap}}$
EOS	equation of state
k	Boltzmann's constant

LJ	Lennard-Jones
max AD%	maximum absolute-value percent relative deviation $= \max_{i=1}^{NP} 100 \lvert P_{model}^{vap} - P_{exp}^{vap} \rvert / P_{exp}^{vap}$
N_A	Avogadro's number
NP	number of data points
P	absolute pressure
P_c	critical pressure
P_r	practical reduced pressure $= P/P_c$
P^{vap}	vapor pressure
P_{SFE}^{+}	LJ melting P^+
r	intermolecular distance
T	absolute temperature
T_c	critical temperature
T_r	practical reduced temperature $= T/T_c$
u	potential energy
z	compressibility factor

Greek letters

ε	depth of the LJ potential well
$\rho_{fluid,SFE}^{+}$	dimensionless density of the dense LJ fluid in equilibrium with the LJ solid
ρ	mole density
ρ_c	critical mole density
σ	LJ separation distance at zero energy

Acknowledgements

The authors are indebted to the European Commission (EVIDENT project, contract No. JOF3-CT97-0034), for financial support, and to Consejo Nacional de Investigaciones Científicas y Técnicas de la República Argentina.

Appendix A. The assumption of constant residual pressure

A conventional linear scheme for pressure extrapolations in temperature would be the following.

$$P^+ = P_{ref}^+ + (P^+)'_{T_{ref}^+}(T^+ - T_{ref}^+) \tag{A.1}$$

where $(P^+)'_{T_{ref}^+}$ is the partial derivative $\partial P^+/\partial T^+$ evaluated at T_{ref}^+ and at ρ^+. When the ideal gas state is approached, i.e. when density tends to 0, the derivative $(P^+)'_{T_{ref}^+}$ tends to ρ^+. Hence, Eq. (15) of the text can be seen as a conventional linear extrapolation scheme in temperature, simplified through approximating the derivative $(P^+)'_{T_{ref}^+}$ with its ideal gas expression.

Table 3
Parameters for Eqs. (B.2) and (B.3)

	Range of applicability	
	$26.792 \geq X \geq 1.913714$, $0.05 \leq T^+ \leq 0.7$	$1.913714 \geq X \geq 1$, $0.7 \leq T^+ \leq T_c^+$ ($T_c^+ = 1.3396$)
Eq. (B.2)		
C_1	-3.9861939990000000	-3.9861948470775700
C_2	-2.6866929859013500	-4.6375884689076900
C_3	$-3.4972762407717100 \times 10^{-4}$	$-3.6134532060524600 \times 10^{-1}$
C_4	$6.5754749882896100 \times 10^{-4}$	$1.4119528267359000 \times 10^{-2}$
C_5	$-1.1469464793808900 \times 10^{-4}$	$1.3876184735954800 \times 10^{-2}$
C_6	$9.6938574173793900 \times 10^{-6}$	$-1.0492074195993400 \times 10^{-1}$
C_7	$-4.4395676013937400 \times 10^{-7}$	$-7.3871672162542300 \times 10^{-2}$
C_8	$1.0436731563233000 \times 10^{-8}$	$-4.7043694762065000 \times 10^{-2}$
C_9	$-9.3439364960073900 \times 10^{-11}$	$5.6137946063172200 \times 10^{-3}$
C_{10}	$-1.6577015678260900 \times 10^{-13}$	$6.0199517668712400 \times 10^{-5}$
C_{11}	1.9137143	1.9137143
Maximum error[a] in calculated P^+ (%)		
	0.2	3.2×10^{-4}
	Range of applicability	
	$2.442823 \times 10^{-31} \leq Y \leq 1.857077 \times 10^{-2}$, $0.05 \leq T^+ \leq 0.7$	$1.857077 \times 10^{-2} \leq Y \leq 1$, $0.7 \leq T^+ \leq T_c^+$ ($T_c^+ = 1.3396$)
Eq. (B.3)		
D_1	1.9137142875511800	1.9137142875511800
D_2	$-3.7226684284862000 \times 10^{-1}$	$-2.1562205993968200 \times 10^{-1}$
D_3	$-2.0402808070806900 \times 10^{-5}$	$-3.6652371328205900 \times 10^{-3}$
D_4	$-1.1893931236856300 \times 10^{-5}$	$-6.6675577354054800 \times 10^{-5}$
D_5	$-7.5424792709156900 \times 10^{-7}$	$-8.9386803365887000 \times 10^{-5}$
D_6	$-2.3817194433494600 \times 10^{-8}$	$6.2728933498223300 \times 10^{-5}$
D_7	$-4.1521399113226400 \times 10^{-10}$	$-1.8028612925501300 \times 10^{-5}$
D_8	$-3.7155915735425500 \times 10^{-12}$	$3.3474928821195800 \times 10^{-6}$
D_9	$-1.1686049441009600 \times 10^{-14}$	$-2.0957624312109200 \times 10^{-7}$
D_{10}	$1.9676957115858100 \times 10^{-17}$	$-5.8182590872080500 \times 10^{-10}$
D_{11}	-3.986193999	-3.986193999
Maximum error[a] in calculated T^+ (%)		
	6.0×10^{-3}	7.5×10^{-5}

[a] With respect to the iterative procedure.

Appendix B. Definitions of $F_{\mathbf{dir}}$ and $F_{\mathbf{inv}}$

Definition of F_{dir}

$$Y = F_{\mathrm{dir}}(X) = \exp(U_{\mathrm{dir}}) \tag{B.1}$$

$$U_{\mathrm{dir}} = C_1 + \sum_{i=2}^{10} C_i (X - C_{11})^{(i-1)} \tag{B.2}$$

Definition of F_{inv}

$$X = F_{\text{inv}}(Y) = D_1 + \sum_{i=2}^{10} D_i (\ln Y - D_{11})^{(i-1)} \tag{B.3}$$

The constants C_i and D_i are given in Table 3. These constants are general for the EXT-LJ-EOS.

References

[1] J.M. Prausnitz, R.N. Lichtenthaler, E. Gomes de Azevedo, Molecular Thermodynamics of Fluid-Phase Equilibria, 3rd Edition, Prentice-Hall, New Jersey, 1999 (Chapter 4).

[2] T.F. Sun, J. Bleazard, A.S. Teja, A method for the prediction of the transport properties of dense fluids: application to liquid *n*-alkanes, J. Phys. Chem. 98 (1994) 1306–1310.

[3] R.C. Reid, J.M. Prausnitz, B.E. Poling, The Properties of Gases and Liquids, 4th Edition, McGraw-Hill, New York, 1988 (Chapter 9).

[4] T. Sun, A.S. Teja, Vapor–liquid and solid–fluid equilibrium calculations using a Lennard-Jones equation of state, Ind. Eng. Chem. Res. 37 (1998) 3151–3158.

[5] R. L Rowley, M.M. Painter, Diffusion and viscosity equations of state for a Lennard-Jones fluid obtained from molecular dynamics simulations, Int. J. Thermophys. 18 (1997) 1109.

[6] M.S. Zabaloy, J.M.V. Machado, E.A. Macedo, A study of Lennard-Jones equivalent analytical relationships for modeling viscosities, Int. J. Thermophys. (2001), in press.

[7] O. Pfohl, Evaluation of an improved volume translation for the prediction of hydrocarbon volumetric properties, Fluid Phase Equilib. 163 (1999) 157–159.

[8] J. Kolafa, I. Nezbeda, The Lennard-Jones fluid: an accurate analytic and theoretically-based equation of state, Fluid Phase Equilib. 100 (1994) 1–34.

[9] J.K. Johnson, J.A. Zollweg, K.E. Gubbins, The Lennard-Jones equation of state revisited, Mol. Phys. 78 (1993) 591.

[10] M. Mecke, A. Müller, J. Winkelmann, J. Vrabec, J. Fischer, R. Span, W. Wagner, An accurate Van der Waals-type equation of state for the Lennard-Jones fluid, Int. J. Thermophys. 17 (1996) 391; also Erratum 1 in Int. J. Thermophys. 19 (1998) 1493.

[11] R. Agrawal, D.A. Kofke, Thermodynamic and structural properties of model systems at solid–fluid coexistence. II. Melting and sublimation of the Lennard-Jones system, Mol. Phys. 85 (1995) 43–59.

[12] M.S. Zabaloy, J.H. Vera, Cubic equation of state for pure compound vapor pressures from the triple point to the critical point, Ind. Eng. Chem. Res. 35 (1996) 829–836.

[13] R.J. Topliss, D. Dimitrelis, J.M. Prausnitz, Computational aspects of a non-cubic equation of state for phase-equilibrium calculations. Effect of density-dependent mixing rules, Comput. Chem. Eng. 12 (1988) 483–489.

[14] J.M. Mollerup, M.L. Michelsen, Calculation of thermodynamic equilibrium properties, Fluid Phase Equilib. 74 (1992) 1.

[15] G. Soave, Direct calculation of pure-compound vapour pressures through cubic equations of state, Fluid Phase Equilib. 31 (1986) 203–207.

[16] P.A. Sacomani, H.P. Gros, E.A. Brignole, Computation of the attractive energy parameter of normal fluids in cubic equations of state, Fluid Phase Equilib. 122 (1996) 27.

[17] DIPPR 801, Evaluated process design data, Public Release 1998, American Institute of Chemical Engineers, Design Institute for Physical Property Data, BYU-DIPPR, Thermophysical Properties Laboratory, Provo, Utah.

[18] K. Stephan, K. Lucas, Viscosity of Dense Fluids, Plenum Press, New York, 1979.

[19] M.S. Zabaloy, J.H. Vera, Identification of variant and invariant properties in the thermodynamics of mixtures: tests for models and computer codes, Fluid Phase Equilib. 119 (1996) 27–49.